



Electrodeposition and characterization of copper sulfide (CuS) thin film: towards an understanding of the growth mechanism

A. Ait-karra¹ · O. Zakir^{1,2} · A. Ait baha¹ · M. Lasri¹ · R. Idouhli¹ · M. Elyaagoubi² · A. Abouelfida¹ · M. Khadiri¹ · J. Benzakour¹

Received: 21 November 2022 / Revised: 13 March 2023 / Accepted: 13 March 2023 / Published online: 24 March 2023
© The Author(s), under exclusive licence to Springer-Verlag GmbH Germany, part of Springer Nature 2023

Abstract

Copper sulfide (CuS) thin film was electrodeposited onto stainless steel (SS 316L) substrate under pulse potential control, from an aqueous acidic solution containing 10^{-3} M of $\text{CuSO}_4 \cdot 5\text{H}_2\text{O}$ and 10^{-2} M of $\text{SC}(\text{NH}_2)_2$. The solution pH was maintained at 2.2 ± 0.1 by adding a few microliters of 0.1 M H_2SO_4 solution. The electrodeposited thin film was grown at 30 °C by applying a forward potential (E_F) of -0.85 V vs Ag/AgCl for 0.2 s and a reverse potential (E_R) of 0 V vs Ag/AgCl for 0.4 s. Cyclic voltammetry (CV) was used to determine E_F and E_R as well as the possible reactions that occurred in the studied system and to understand the electrochemical behavior of the SS 316 L substrate on the deposition solutions. Normal and grazing incidence X-ray diffraction (XRD), Raman spectroscopy, and energy-dispersive analysis of X-ray (EDAX) techniques showed that the obtained thin film, applying E_F and E_R , was a hexagonal covellite CuS. Scanning electron microscopy (SEM) analysis showed that the obtained CuS film is grainy and contained some cracks. Profilometry indicated that the elaborated film has a thickness of 7.85 ± 0.71 μm . Electrochemical impedance spectroscopy (EIS) and Mott–Schottky (MS) analysis were performed, but the results are controversial because of the participation of SS 316 L substrate in the behavior of the obtained data.

Keywords CuS · Pulse electrodeposition · Growth mechanism · Thin film · Cyclic voltammetry · Mott–Schottky

Introduction

Thin film materials have become a crucial topic of research in the last few decades, because of their potential use in electrical and optical devices [1, 2]. Among thin film materials, metal sulfides with their promising optical and electrical properties have attracted a great deal of research attention during this period [3]. Recent efforts have been focused on the elaboration and study of metal sulfides such as cadmium sulfide [3], zinc sulfide [4], cobalt sulfide [5], manganese sulfide [6], tin sulfide [7], and copper sulfide [8]. Most of these latest materials have shown some toxicity;

however, the relatively low toxicity and the abundance of copper sulfide make it a great candidate for the scientific research. Copper sulfide with the formula (Cu_xS) has four stable phases at room temperature; it can be obtained rich in copper such as *chalcocite* (Cu_2S), *djurlite* ($\text{Cu}_{1.95}\text{S}$), and *anilite* ($\text{Cu}_{1.75}\text{S}$), or rich in sulfur such as *covellite* (CuS) [9]. This material represents one of the most important semiconducting transition metal sulfides, because of their unique physical and chemical properties [10, 11]. The research on copper sulfide was initiated with the discovery of the photovoltaic effect in the $\text{CdS}-\text{Cu}_x\text{S}$ heterojunction solar cell [12]. Among the copper sulfide phases, the covellite CuS is considered a multifunctional material because of its wide area of use [13]. It was developed as an optical filter [14, 15], absorber, and controller in solar cells [16, 17], catalyst [18, 19], material for lithium-ion batteries [20, 21], supercapacitors [7, 22], sensors [23, 24], thermoelectric materials [25, 26], and so on.

The large area of application was driving researchers to prepare the covellite CuS, study its physicochemical properties, and dedicate it to new applications. For this reason,

✉ A. Ait-karra
a.aitkarra@gmail.com

¹ Chemistry Department, Faculty of Science Semailia, Applied Chemistry and Biomass Laboratory, Cadi Ayyad University, BP 2390 Marrakech, Morocco

² Department of Physics, Faculty of Science Semailia, Laboratory of Nanomaterials for Energy and Environment, Cadi Ayyad University, BP 2390 Marrakech, Morocco

various elaboration techniques have been developed to synthesize this material such as chemical bath deposition (CBD) [27], chemical vapor deposition (CVD) [28], spray pyrolysis [29], thermal co-evaporation [30], microwave [31], wet chemical [32], sonochemical [33], solvothermal [34], hydrothermal [35], sol–gel [36], microemulsion [37], and electrodeposition techniques [17]. As a result of this diversity, the covellite CuS was obtained with various morphologies such as nanoflakes [38], nanotubes [39], microspheres [40], nanorods [41], nanoparticles [42], nanowires [43], nanoribbons [44], flower-like structures [45], and urchin-like structures [46].

Among the elaboration techniques, the electrodeposition method has been used as an easy and simple method to prepare good-quality thin films [47]. This method is preferred for the elaboration of reproducible thin films, because of the following reasons: It is easily scalable and inexpensive, it could be used over a large area, and it enables accurate control over composition, growth direction, and growth size. Also, it is very favorable because of its simplicity and repeatability [7, 43, 48]. This technique can be done by potentiostatic, galvanostatic, and pulsed potential or pulsed current modes, and in two- or three-electrode electrochemical cells [49, 50]. There have been many studies on the electrodeposition synthesis of CuS thin films. Thanikaikarasan et al. have obtained CuS thin film onto indium-doped tin oxide-coated conducting glass (ITO) substrates from an aqueous acidic bath containing CuSO_4 , $\text{Na}_2\text{S}_2\text{O}_3$, and EDTA, via potentiostatic mode by applying of -0.5 V versus SCE, and the temperature range of was between 45 and 75 °C [51]. Dhasade et al. have synthesized CuS nanorods at room temperature onto ITO substrates from the aqueous acidic bath containing CuSO_4 , $\text{Na}_2\text{S}_2\text{O}_3$, and TEA, via potentiostatic mode by applying -0.7 V versus SCE [17]. Sarma et al. and Ghahremaninezhad et al. have prepared CuS thin film onto platinum (Pt) foil from an aqueous acidic bath containing CuSO_4 and thiourea, using pulsed potentiostatic mode by applying $E_F = -0.85$ V followed by $E_R = 0$ V vs Ag/AgCl for forward and reverse durations, respectively [8, 52].

According to our knowledge, no works were performed to obtain copper sulfide on SS 316 L substrate using the pulse electrodeposition method. The novelty and originality of this work are to get CuS thin film onto SS 316 L working electrode using pulsed potentiostatic electrodeposition mode at low temperature. The choice of this substrate was based on its availability, low price, nontoxicity, and the poor experimental results obtained by using FTO as the working electrode. The use of pulse electrodeposition mode was based on the results obtained by the potentiostatic mode (fixation of a single cathodic potential). In addition, the majority of works performed on CuS thin film were carried out with platinum (Pt), gold (Au), and ITO or FTO, while these substrates are too expensive compared to stainless steel. As either as it is

declared above, the aim of this paper is to prepare the covellite CuS thin film using electrochemical deposition. The deposition solution was an aqueous acidic mixture of copper sulfate CuSO_4 and thiourea $\text{SC}(\text{NH}_2)_2$. The choice of the deposition potentials of CuS and the determination of the possible reactions in the studied system were examined using cyclic voltammetry (CV) and pulse electrodeposition studies. The obtained black film was annealed at 200 °C for 5 h, before being characterized. The final product was analyzed using X-ray diffraction (XRD), Raman spectroscopy, and scanning electron microscopy (SEM) coupled with the energy dispersive X-ray (EDAX). The thickness of the obtained CuS film was determined using profilometry and SEM analysis. The electrochemical studies were carried out to model the film/electrolyte interface and to determine the semiconducting nature of the prepared film.

Experimental procedure

Electrochemical elaboration

The elaboration of CuS film was carried out in a conventional three-electrode system comprising platinum (Pt) foil as a counter electrode (C.E), stainless steel (SS 316 L) plate, or fluorine-doped tin oxide (FTO)-coated glass substrates as a working electrode (W.E), and the saturated silver/silver chloride (Ag/AgCl) as a reference electrode (R.E). The elaborated films were grown at 20, 30, and 40 °C, from an aqueous acidic bath containing 10^{-3} M of copper sulfate pentahydrate ($\text{CuSO}_4 \cdot 5\text{H}_2\text{O}$) and 10^{-2} M of thiourea ($\text{SC}(\text{NH}_2)_2$). The pH of the deposition solution was adjusted to 2.2 ± 0.1 by sulfuric acid (H_2SO_4) solution. The electrochemical measurements were performed using Radiometer Voltalab PGZ 301 potentiometer, and all measured potentials cited in the experimental procedure part are related to R.E. Prior to any electrodeposition, the SS plates are prepared by polishing with different emery paper sizes (from #2000 to #5000 grade) until a surface like a mirror was obtained, then rinsed with distilled water, and degreased by sonication in ethanol [53]. After that, the back and the edges of the substrate are covered by a layer of varnish to avoid local peak fields at the electrodes and also to stare the exposed surface [54]. FTO substrates were washed in a mixture of water and a liquid soap. After that, they were transferred successively in two baths consisting of water/ethanol and water/acetone in an ultrasonic device [54]. Before the electrodeposition process, a cyclic voltammetry (CV) study was carried out in the cell declared above in order to determine the deposition potentials and to get an idea of the possible reactions in the studied system. During electroplating, the evolution of potential and current density against time was recorded.

After electroplating, the obtained film was annealed at 200 °C in ambient air for 5 h.

Physicochemical characterization

The crystalline structure of the obtained film was characterized by normal and grazing incidence X-ray diffraction (XRD) using a Rigaku, SmartLab SE, operated at 40 kV and 50 mA. The X-ray source consists of Cu K α radiation (1.54184 Å) selected with a Cu K β filter. The diffractograms were collected between 20 and 80° with a scan rate of 5°/min. Raman spectroscopy was also used to characterize the prepared film by determining the functional groups and their vibrations. The Raman spectrums were collected between 200 and 600 cm⁻¹, by a confocal Raman spectrometer (Confotec MR520 microscope) instrument with a laser ($\lambda = 532$ nm) and analyzed with a grating of 1200 lines/mm. The morphology of the prepared film was analyzed by scanning electron microscopy (SEM) using a field emission scanning electron microscope (TESCAN VEGA3 SEM). The chemical composition of the sample was determined with an energy-dispersive microanalysis of the X-ray system (EDAX) coupled with SEM and operated at an accelerating voltage of 20 kV. The film thickness was evaluated using a DektakXT Bruker profilometer.

The electrochemical impedance spectroscopy (EIS) and Mott–Schottky (MS) measurements were performed in a conventional three-electrodes cell containing a platinum (Pt) foil as a counter electrode (surface area = 2 cm²) and Ag/AgCl (KCl-saturated solution) as a reference electrode in a 10⁻¹ M Na₂SO₄ aqueous solution [53]. The CuS film obtained onto stainless steel (surface area = 1 cm²) was used as a working electrode. All measurements were carried out at 25 °C and performed using Radiometer Voltalab PGZ 301 potentiometer controlled by the VoltaMaster 4 software. For EIS, the study was performed at the frequency range of 100 kHz–10 mHz. The MS study was performed at 1 kHz in the potential range of -0.6 to 0.6 V vs Ag/AgCl.

Results and discussion

Cyclic voltammetry study

In order to determine the suitable deposition potential of CuS and the possible reactions of the studied system, the cyclic voltammetry (CV) technique was used as a great analytical tool for studying the behavior of electrochemical depositions [51]. For this study, four voltammograms were recorded in the potential range of 1 to -1 V with a scanning rate equal to 10 mV/s. These curves are shown in Fig. 1, where (a) is related to the whole voltammograms, (b) is related to their reduction direction, and (c) shows their oxidation direction.

The first study corresponds to the electrochemical behavior of stainless steel (SS) working electrode in an aqueous acidic solution (pH = 2). This study shows one cathodic peak which started from ~ -0.55 to -1 V. In this latest potential range and during the voltammogram (curve (a)) recording, it was observed at the surface of SS an appearance of gas bubbles which can be attributed to the reduction of H⁺ ions to H₂ gas according to the global reaction (1) [8]. From the same voltammogram, it was also observed an anodic peak at around -0.07 V which can be due to the oxidation of SS followed by passivation.



In literature, the electrochemical behavior of thiourea (TU) was discussed and published by Kang et al. The authors have studied the complexing effect of TU on copper electrodeposition. They showed that TU intervenes as a complexing agent of Cu²⁺ and Cu⁺ ions, slows down the copper deposition, and does not reflect any electrochemical reaction [55]. The third voltammogram (curve (b)) is relevant for the electrochemical behavior of SS in 10⁻² M of TU solution (pH = 2). This study shows that TU is electrochemically inactive in the chosen potential range, and its voltammogram is confused with that obtained in the first cyclic voltammetry study (curve (a)). This shows that the only detected effect is due to the electrochemical behavior of the H⁺/H₂ system, with an insignificant difference in the reduction potential of H⁺ ions, which is moved towards the cathodic direction. In addition, the electrochemical activity of the SS substrate was also detected at around -0.07 V.

The curve (c) shows the electrochemical behavior of SS in 10⁻³ M of CuSO₄ solution. It revealed that the cathodic current decreases gradually from ~ -0.112 to ~ -0.55 V vs Ag/AgCl. The observed strong peak (C₁) at ~ -0.55 V is attributed to the reduction of Cu²⁺ to Cu⁺ and also Cu⁺ to metallic copper according to reactions (2) and (3) respectively. Another quick decrease of the cathodic current was detected from ~ -0.85 to -1 V vs Ag/AgCl, which refers to the reduction of H⁺ ions to H₂ gas. In the oxidation part of the voltammogram, two anodic peaks A₁ and A₂ were observed. The first one (A₁) at ~ 0.29 V corresponds to the oxidation of metallic copper to Cu⁺ according to the inverse of reaction (3), whereas the second one (A₂) at ~ 0.465 V relates to the oxidation of Cu⁺ to Cu²⁺ according to the opposite of reaction (2) [8, 51, 52]. It was also observed a disappearance of the oxidation peak of SS, which may be due to the formation of a copper film on the SS surface.



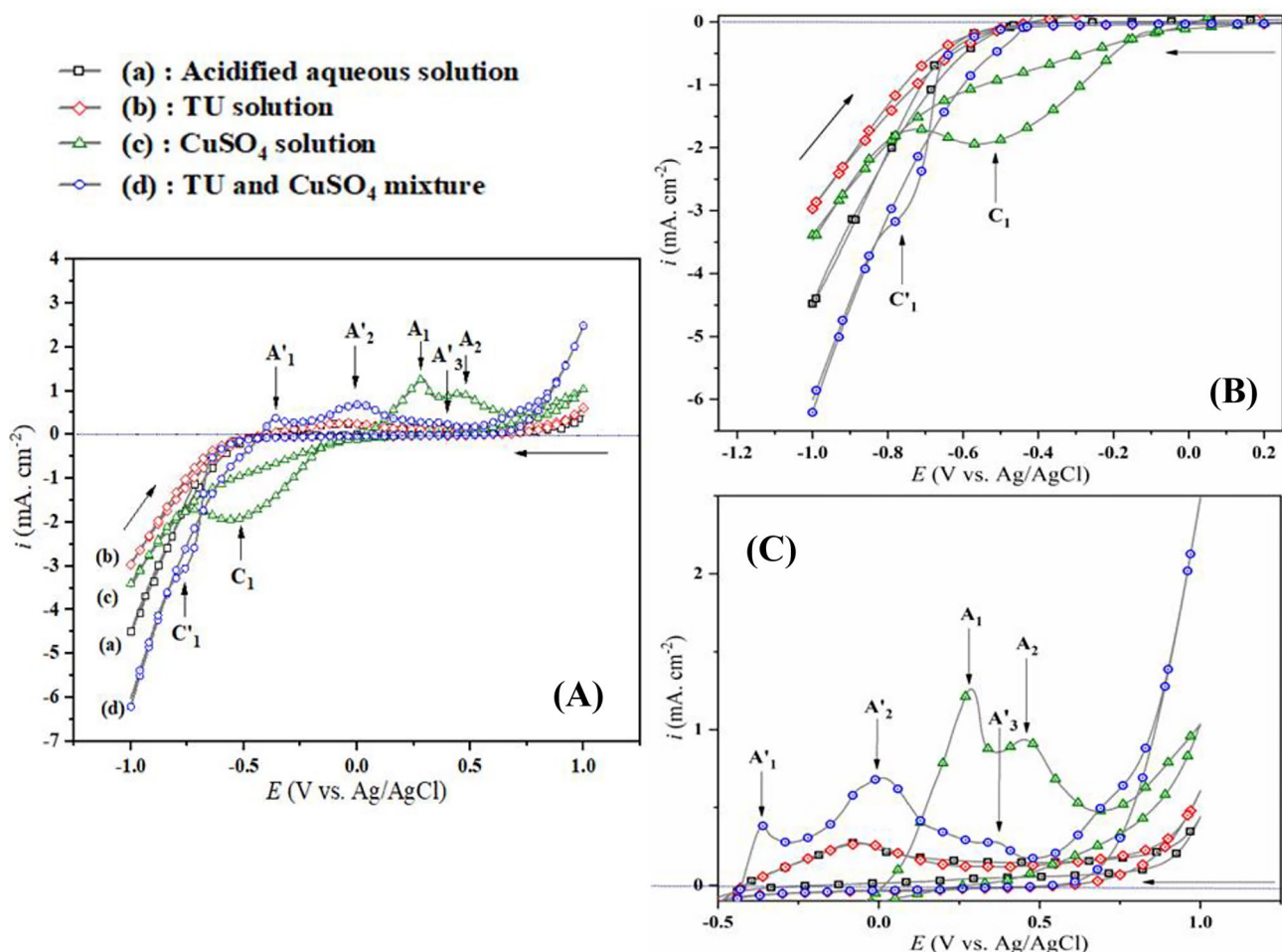
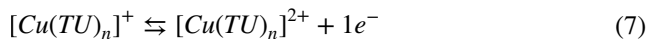
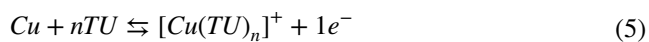
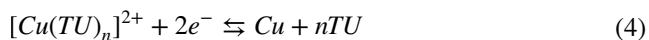


Fig. 1 CV curves indicating the electrochemical behavior of SS 316 L in different solutions: Full cyclic voltammograms (A), reduction direction (B), and oxidation direction (C)

The electrochemical behavior of SS in the mixture of 10^{-3} M of CuSO_4 and 10^{-2} M of TU (pH=2) at 30°C is represented by the curve (d) of Fig. 1. Firstly, the global current density decreases algebraically showing the participation of TU in the global current density. Secondly, the cathodic current density starts to decrease slowly from ~ -0.25 to ~ -0.65 V, this observation can be attributed to the reduction of the free Cu^{2+} cations to metallic copper. After that, a quick decrease of the cathodic current density starts from ~ -0.65 to -0.85 V and leads to the C'_1 peak. This phenomenon can be attributed to the reduction of Cu^{2+} cations complexed by TU to metallic copper and TU according to reaction (4). It is observed from the same voltammogram a quick decrease of the cathodic current from ~ -0.85 to -1 V, and this observation is due to the reduction of H^+ ions to H_2 gas [51, 52]. In the oxidation direction, three anodic peaks were observed A'_1 , A'_2 , and A'_3 at ~ -0.36 V, ~ 0 V, and ~ 0.38 V respectively. The A'_1

may be attributed to the reaction of metallic Cu with TU according to reaction (5) [8, 52], or to the oxidation of the electrodeposited copper on the SS working electrode. The A'_2 refers to an activation of the SS substrate in the deposition solution. It is observed from the same voltammogram that the A'_2 has gained in terms of intensity compared to the case of pristine SS. This difference is attributed to the oxidation of metallic copper with TU to CuS according to reaction (6). This latest is a global reaction which passes through an intermediate state, in which copper oxidizes to Cu^{2+} and TU decomposes to S, NH_4^+ , and CN^- . In addition, similar reactions were proposed for nickel sulfide (NiS) and zinc sulfide (ZnS) electrodeposition using TU as a precursor of sulfur [56, 57]. The small A'_3 peak can be assigned to the oxidation $[\text{Cu}(\text{TU})_n]^+$ to $[\text{Cu}(\text{TU})_n]^{2+}$ according to reaction (7) [8, 52]. The displacement of peak activity towards the cathodic direction and the decrease in current density can be due to the complexing effect of TU.



From this study, it seems that CuS cannot be obtained by applying a fixed cathodic potential, due to the reduction part of the voltammogram of the studied system that has only shown the deposition of metallic copper onto the SS substrate. This hypothesis was proved by EDAX analysis which revealed that the obtained films using cathodic potentiostatic electrodeposition were completely composed of copper. However, the obtention of CuS onto SS using the electrodeposition technique should pass through more than one step. Our conclusion is in good agreement with the literature [52].

Study of the electrodeposition modes

To prepare CuS onto stainless steel and FTO substrates using cathodic potential electrodeposition, different cathodic potentials are applied at different times. The choice of the cathodic applied potential was based on the CV studies. For each substrate, we have applied -0.55 V, -0.65 V, -0.75 V, -0.85 V, and -1 V vs Ag/AgCl during different times greater than 30 min. The obtained films using this mode were red-brown. After characterization, EDAX analysis has shown that the atomic percentage of copper was greater than the atomic percentage of sulfur (practically no sulfur on the surface). Raman analysis did not show any characteristic peak of CuS. It was also observed from this analysis that the obtained films have a metallic behavior (intensity against Raman shift was a horizontal line). However, synthesizing CuS using this mode seems to be impossible. For this reason, we switched to the pulsed potential mode.

The pulsed potential mode consists in fixing two successive potentials E_F and E_R during t_F and t_R respectively. Figure 2 shows the variation of potential (E) and current

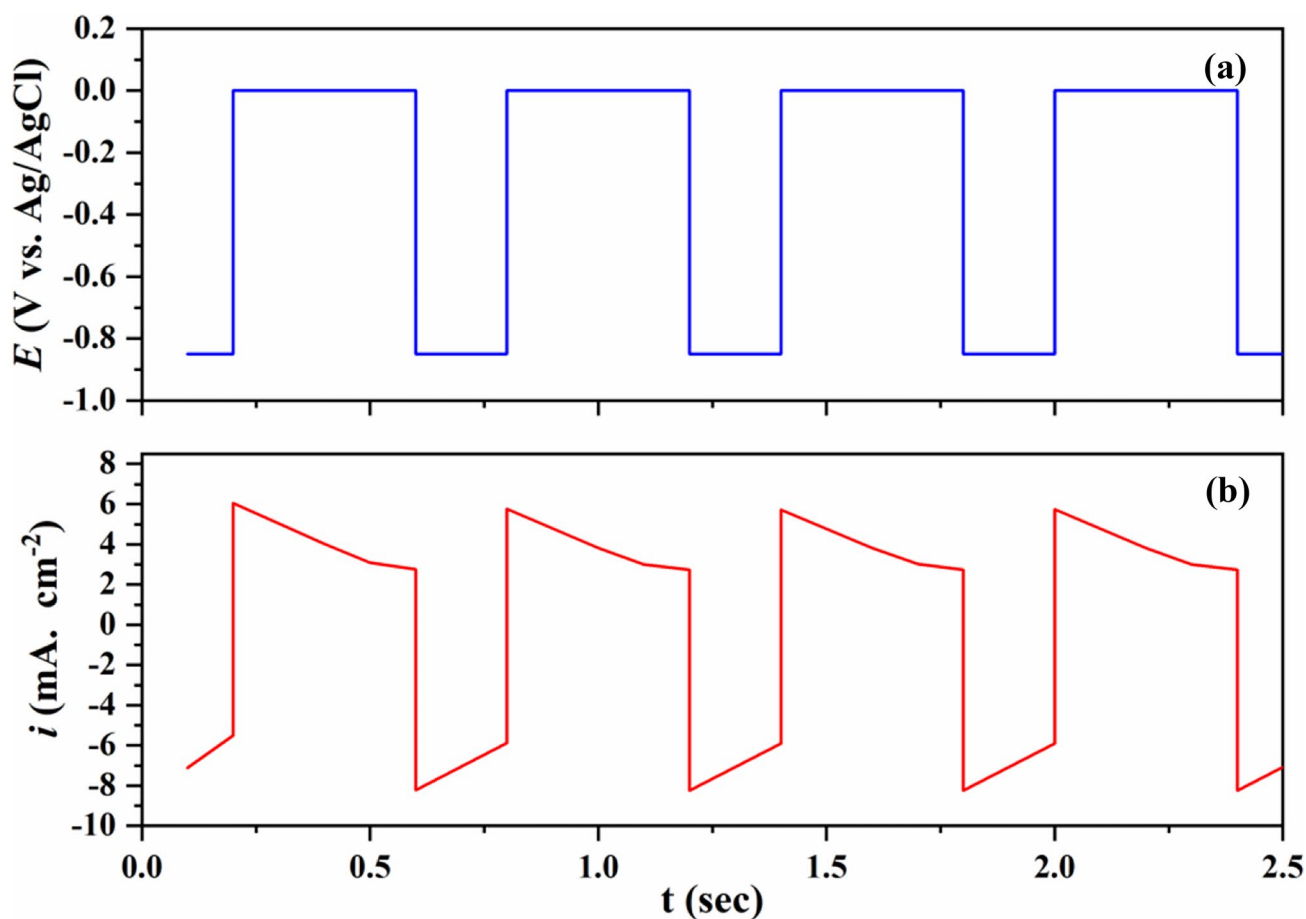


Fig. 2 Variation of potential (a) and current density (b) against time during the pulse electrodeposition process

density (i) against time (t) during the elaboration of CuS onto the SS substrate. During this process, the forward potential ($E_F = -0.85$ V) was applied for $t_F = 0.2$ s and the reverse potential ($E_R = 0$ V) was applied for $t_R = 0.4$ s. The application of E_F consists in depositing of copper onto SS according to reaction (4). In contrast, the application of E_R consists in the formation of CuS or copper-thiourea complex and the dissolution of a part of electrodeposited metallic copper. The variation of E against t is shown in Fig. 2a. From this figure, this variation remains the same for each cycle and during the whole elaboration process. As it is reported in the literature, the application of -0.85 V corresponds to the electrodeposition of copper onto SS. While, the application of 0 V consists in the electrodeposition of copper sulfide, with some adsorbed organic species coming from the decomposition thiourea and the dissolution of a part of copper deposited before [8]. Figure 2b shows the variation of i against t . In this figure, we distinguish two successive peaks. The first one is a cathodic peak current density of ~ -8 mA \cdot cm $^{-2}$; it appears when E_F is applied and it indicates the reduction of Cu^{2+} cations complexed by TU to metallic copper and TU according to reaction (4). The second one is an anodic peak current density of ~ 6 mA \cdot cm $^{-2}$; it appears when E_R is applied, and it indicates the reaction of metallic Cu with TU according to reaction (6) or the dissolution of the electrodeposited metallic copper. These results are in agreement with CV results and those reported in the literature [8]. These variations remain the same during the electrodeposition process, which lasted 3 h divided into 1 h of applying E_F and 2 h of applying E_R . After that, pure CuS was obtained by annealing at 200 °C in the ambient air for 5 h.

After the failure to obtain CuS on the FTO substrate by cathodic electrodeposition mode and the success in getting this material on the SS substrate by pulse electrodeposition, we tried to synthesize this compound on FTO by pulse electrodeposition. During the elaboration process, the current density against time became stable at 0 mA/cm 2 after 3–5 min maximum, whatever the value of the applied potential. Consequently, the FTO substrate remains without any deposited film whatever the duration of the electrodeposition at 30 °C. According to our knowledge, CuS was obtained on ITO and FTO substrates using cathodic electrodeposition mode at a temperature higher than 45 °C [51] and at room temperature [58] which is contradictory to our results. In addition, no studies have addressed the obtaining of CuS onto this substrate (FTO) by the pulsed mode. Therefore, the FTO substrate remains a bad choice for CuS electrodeposition at the applied experimental conditions.

X-ray diffraction analysis

X-ray diffraction (XRD) analysis was used to determine the nature of the electrodeposited film and its crystalline structure. For this reason, two measurements of XRD modes were

carried out. The first one is Bragg–Brentano mode and the second one is X-reflectivity mode (grazing incidence X-ray diffraction). Figure 3 shows the diffractogram of the electrodeposited and annealed film recorded by the first mode. It is observed from this figure that the peaks associated with the substrate (stainless steel) are dominant and hide the peaks of the electrodeposited and annealed sample. In addition, the peaks related to the substrate have lost in intensity 10 times compared to the case of the substrate without deposit. From these remarks and basing on the results revealed by Mott–Schottky and electrochemical impedance spectroscopy, it can be said that the formed film may have a low thickness. As claimed above, the small peaks indicate the formation of a film. These peaks are located at 2θ values around 28.65° , 31.71° , 37.54° , 44.59° , 47.78° , 56.22° , 63.96° , 67.29° , and 72.69° which may be attributed respectively to the (102), (103), (105), (008), (107), (201), (1010), (118), and (208) lattice planes of the CuS hexagonal phase according to standard JCPDS sheets (JCPDS Card No. 06–0464 and JCPDS Card No 75–2236). These results are in agreement with those reported in the literature [10, 17, 58, 59].

To make sure that the prepared film corresponds to the covellite CuS, the electrodeposited and annealed sample was characterized using grazing incidence X-ray diffraction. Figure 4 shows the grazing X-ray diffractogram of the obtained sample before and after annealing. In this figure (Fig. 4), we observed the presence of four peaks located respectively at 2θ values around 27.83° , 29.37° , 31.69° , and 32.93° which may be attributed to (101), (102), (103), and (006) reticular planes of the CuS hexagonal phase according to standard JCPDS sheets (JCPDS Card No. 06–0464 and JCPDS Card No 75–2236). From

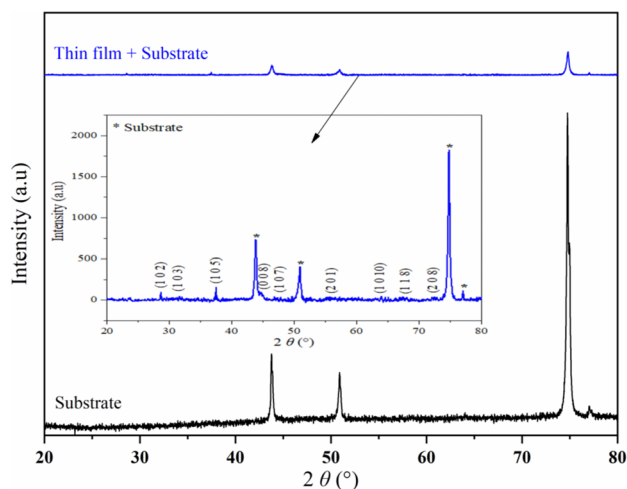


Fig. 3 Normal XRD diffractogram of the as-prepared film onto a stainless steel substrate

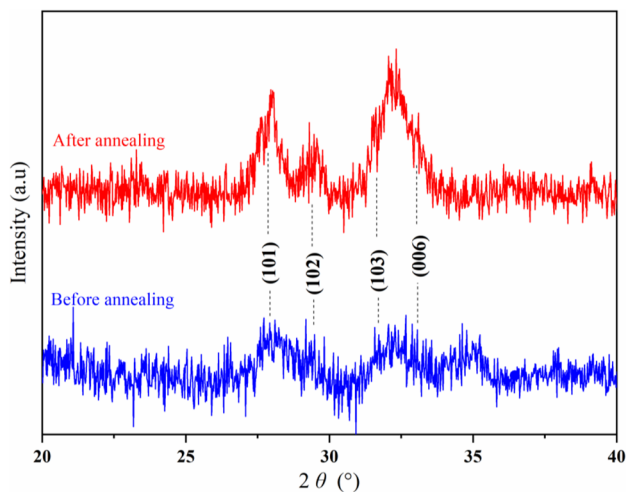


Fig. 4 Grazing incidence XRD patterns of the obtained film onto the SS substrate before and after annealing

the same figure, we note that the peaks have gained in terms of intensity in the case of the sample after annealing, and it was also observed a shifting at 2θ values which may be due to the vacancies in the CuS lattice, created during the film growth or the grain sizes. These results are in good agreement with those reported in the literature [4, 34, 59, 60].

Raman analysis

Raman spectroscopy is an efficient analytical technique for the study of crystal structure within thin solid films [61]. A survey of the literature demonstrates many research works that have been attached to the Raman analysis of CuS film. In our case, the Raman spectrums of the as-prepared sample onto stainless steel substrate before (a) and after (b) annealing were recorded in the wavelength range $200\text{--}600\text{ cm}^{-1}$ using a laser (532 nm). Figure 5 shows the Raman spectrum of the as-prepared sample before and after annealing. It is observed from this figure two different peaks. A hump between centered at $\sim 270\text{ cm}^{-1}$ and a sharp peak between is located at $\sim 473\text{ cm}^{-1}$. As reported in the literature, the first hump is due to the A_{1g} TO mode, and the sharp peak is identified as the S–S stretching mode of S_2 ions at the $4e$ sites [62, 63]. The high-intensity peaks observed at 473 cm^{-1} may be attributed to the formation of the covellite CuS, by correlation to XRD results. By analogy with some previous work, it was also observed a shifting at wave number values which may be due to the vacancies in the CuS lattice, created during the film growth [17, 58, 63, 64].

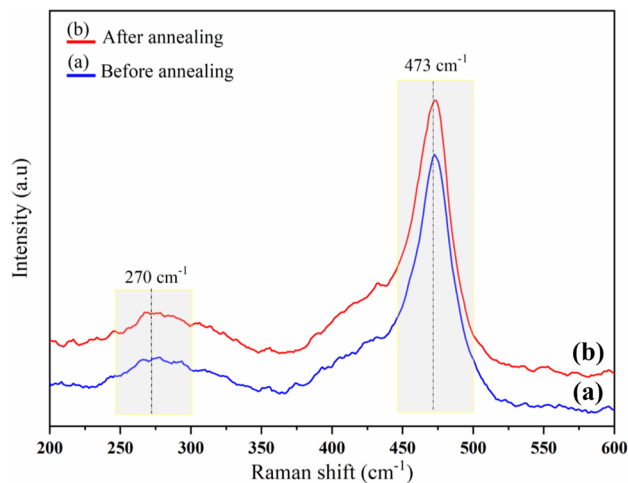


Fig. 5 Raman spectra for the as-prepared film onto SS substrates before (a) and after annealing (b)

Morphological and compositional analysis

The morphological study of the as-prepared sample before and after annealing was carried out using scanning electron microscopy (SEM). Figure 6 shows the SEM micrographs of the as-prepared samples before and after annealing with different resolutions (the total length of the scale bar is $5/10\text{ }\mu\text{m}$ at the left/right images, respectively). The images (a) and (b) are relative to the deposited film before annealing. They indicate that this film is homogenous, formed by spherical grains which are attached to each other and contained some cracks. The observed cracks may be due to the evolution of H_2 gas which is formed at the surface of the substrate (SS 316 L) during pulse electrodeposition. The images (c) and (d) are taken for the prepared film after annealing at $200\text{ }^\circ\text{C}$. It is clear that these images are different from those taken to the film before annealing, in terms of grain size and the number of cracks. In the case of grain size, it is observed that the annealed film is formed by spherical grains on its surface; these grains are agglomerated on the surface of the film by the action of temperature. In addition, it was observed the creation of new cracks in the surface state of the as-prepared film. This creation indicates that the annealing has a strong effect on the morphology of the obtained sample.

To estimate the thickness of CuS film obtained by applying $E_F = -0.85\text{ V}$ for 0.2 s and $E_R = 0\text{ V}$ for 0.4 s at $30\text{ }^\circ\text{C}$, the annealed sample was observed by SEM in a vertical manner. Figure 7 shows the presence of two interfaces which are SS substrate — iron oxides (b) and iron oxides (b) — CuS (a). The thickness of the CuS film was calculated from the obtained SEM image; it was about $9.67 \pm 1.20\text{ }\mu\text{m}$. From the same image, it was observed that the formed

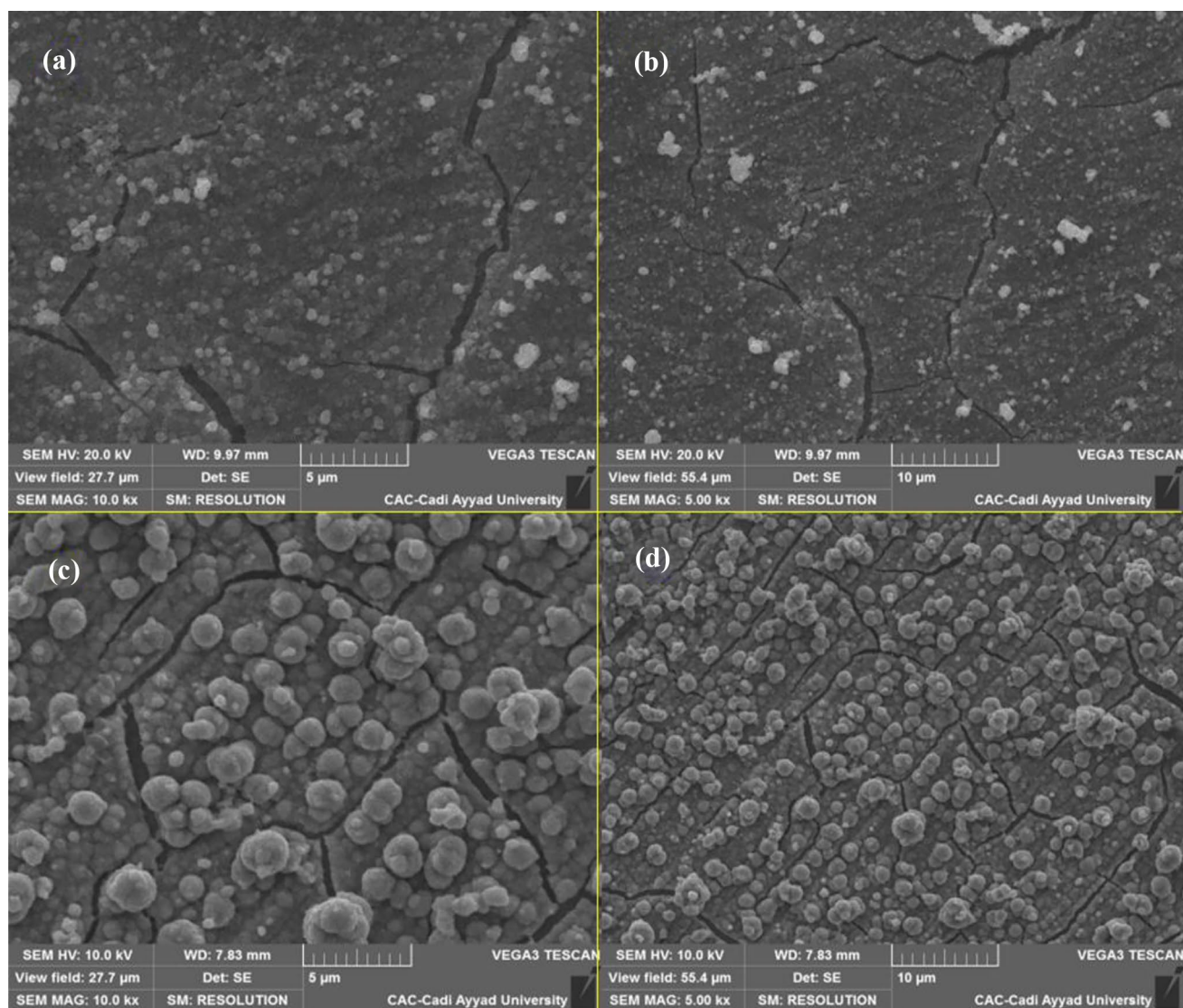


Fig. 6 SEM micrographs of the as prepared film onto SS before (a) and (b) and after (c) and (d) annealing

oxides from the SS substrate have a thickness of about $8.93 \pm 1.40 \mu\text{m}$.

In another way, the thicknesses of the prepared CuS film before and after annealing were evaluated using profilometry. Table 1 summarizes the thickness values of the prepared sample before and after annealing. It indicates that after annealing, the obtained film has lost thickness. This is due to the degradation of organic species adsorbed at the surface of the film. In addition, the thickness of the film obtained after annealing was about $7.85 \pm 0.71 \mu\text{m}$.

In order to determine the mean value and the grain size distribution, a statistical study was carried out on 184 particles selected from the SEM micrograph (resolution $5 \mu\text{m}$) of the film after annealing. This study shows that the majority of the selected particles have a size range between 0.41 and $2.29 \mu\text{m}$, and the average grain size is $1.12 \mu\text{m}$. As it is shown in Fig. 8, the distribution of particle size was fitted to a Gaussian profile.

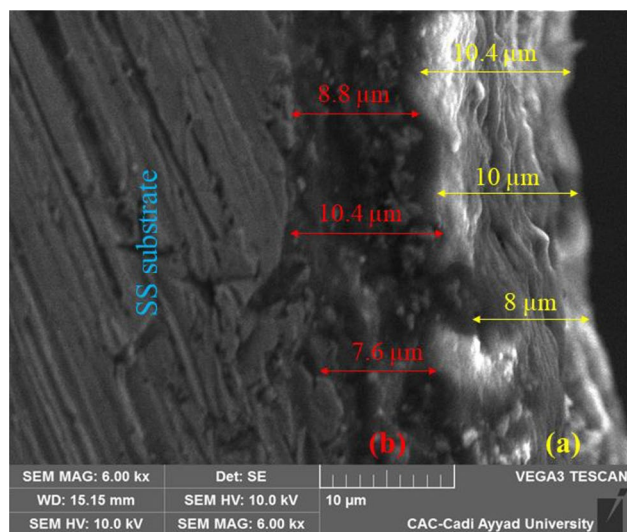


Fig. 7 Thickness of the as-obtained CuS film after annealing

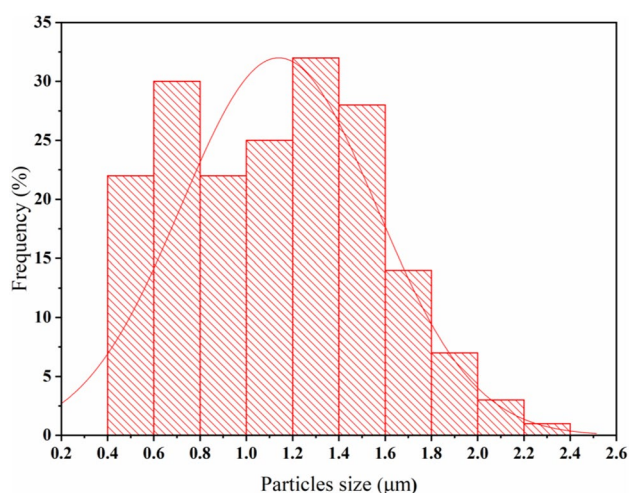
Table 1 Thickness (Th) of the as-prepared thin film before and after annealing

Sample	Th ₁ (μm)	Th ₂ (μm)	Th ₃ (μm)	Average (μm)
Before annealing	14.57	16.40	14.98	15.31
After annealing	7.13	7.85	8.56	7.85

The chemical composition of the electrodeposited samples on SS substrate was evaluated by the energy-dispersive analysis of X-ray (EDAX) technique. Firstly, the effect of temperature on the elemental composition of the as-prepared samples by applying $E_F = -0.85$ V for 0.2 s and $E_R = 0$ V for 0.4 s has been studied between 20 and 40 °C. To evaluate this effect, the three prepared samples at 20, 30, and 40 °C, respectively, were analyzed by EDAX. This technique revealed that the Cu/S ratio closest to unity is obtained for $T = 30$ °C. Table 2 summarizes the elemental composition of the three prepared samples after annealing at 200 °C for 5 h.

Secondly, the effect of the applied potentials on the composition of the obtained sample at 30 °C was determined also by EDAX. Table 3 shows the elemental composition of the as-prepared samples at different applied potentials before annealing. It indicates that the Cu/S ratio closest to unity is obtained by applying $E_F = -0.85$ V and $E_R = 0$ V.

The study of the effects of the temperature and the deposition potentials on the composition of copper sulfide showed that the application of $E_F = -0.85$ V and $E_R = 0$ V at $T = 30$ °C made it possible to obtain a good Cu/S ratio. Figure 9 shows the EDAX spectrum of the electrodeposited film before and after annealing. The EDAX spectrum of the obtained sample before annealing (Fig. 8a) confirms the presence of copper and sulfur with an atomic ratio (Cu/S) equal to 1.08. It is also observed from this figure the existence of many other elements such as iron (Fe), nickel (Ni),

**Fig. 8** Particle size distribution of electrodeposited film onto the SS substrate after annealing**Table 2** Elemental composition of the as-prepared samples at 20, 30, and 40 °C

Sample	Temperature	% Cu	% S	Cu/S
1	20 °C	60.59	39.41	1.53
2	30 °C	52.83	47.17	1.11
3	40 °C	64.90	35.10	1.84

chromium (Cr), and oxygen (O), which are due to the substrate composition (SS 316 L). But the presence of nitrogen (N) and carbon (C) may be attributed to the existence of thiourea or the adsorbed CN^- and NH_4^+ species onto the surface of the film, issued from oxidation of copper following reaction (6).

To remove the intervention of the chemical composition of SS and thiourea or the adsorbed CN^- and NH_4^+ , the obtained film was annealed at 200 °C for 5 h and scraped from the substrate before being characterized. Figure 8b shows the EDAX spectrum of the obtained film after annealing and scraping from the substrate. It is observed from this figure the presence of copper (Cu), sulfur (S), iron (Fe), and oxygen (O) with different atomic percentages. The existence of Cu (43.68%) and S (39.22%) confirms the formation of copper sulfide. While Fe and O indicate the formation of iron oxide from the SS substrate. Through the EDAX spectrum, the atomic ratio of copper and sulfur atoms (Cu/S) is equal to 1.11. This result indicates that the formed copper sulfide is close to being stoichiometric. From this result and by analogy with XRD and Raman analysis, we can see that the obtained film onto stainless steel substrates is the covellite CuS.

Electrochemical analysis

The obtained film/electrolyte interface was studied using the electrochemical impedance spectroscopy (EIS) technique. EIS was carried out in 10^{-1} M Na_2SO_4 solution, with an Ag/AgCl reference electrode and platinum as counter electrode in the frequency range of 100 kHz–10 mHz. Figure 10 illustrates the Nyquist plot of the EIS data obtained for the electrodeposited and annealed sample with its fitting adjustment obtained using the EC-Lab software and the proposed equivalent circuit. The obtained Nyquist plot is similar to those found in the literature [51, 65]. As it is shown in Fig. 10, the Nyquist plot represents a small incomplete semicircle at high frequencies followed by a straight line with a Bode

Table 3 Elemental composition of the as-prepared samples at different applied potentials

Sample	E_F (V)	E_R (V)	% Cu	% S	Cu/S
1	-1	0	47.03	52.97	0.88
2	-0.85	0	51.99	48.01	1.08
3	-0.85	0.15	43.89	56.11	0.78

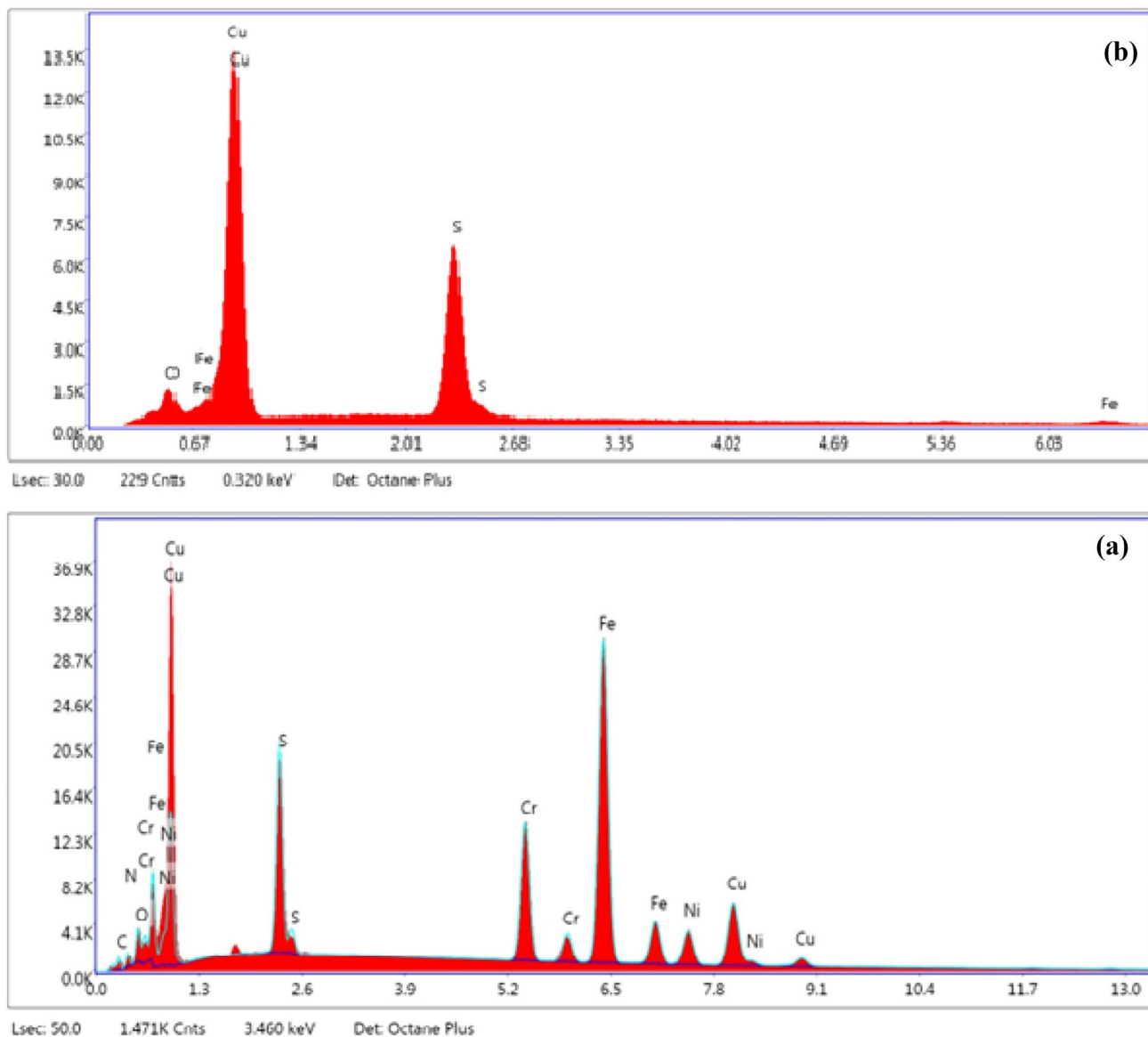


Fig. 9 EDAX spectra of the electrodeposited film before (a) and after (b) annealing

phase angle of $\sim 45^\circ$. Different electrochemical equivalent circuits (EEC) have been proposed to model CuS/electrolyte interface [51, 65, 66]. In our case, the Nyquist plot was adjusted by the following electrochemical equivalent circuit (EEC) as $R_1 + C_2/R_2 + C_3/R_3 + C_4/R_4$ with a good correlation value ($\chi^2 = 6 \times 10^{-3}$). Table 4 summarizes the element values of EEC obtained by fitting of the Nyquist plot of the formed film.

As shown in Fig. 10, the fitted EEC contains an electrolyte resistance element called R_1 in series with a resistance coupled with the capacitance element (R_2/C_2), (R_3/C_3), and (R_4/C_4), corresponding to the porous layer of CuS, the barrier layer of the formed oxides from SS, and the electrochemical double layer. The capacitance elements C_2 , C_3 , and

C_4 are not pure. They have been calculated from constant phase elements (Q_1 , Q_2 , and Q_3) which are used to take into account the surface heterogeneity, nonideality of capacitance, and frequency dispersion [66–68].

Mott–Schottky analysis was carried out in Na_2SO_4 0.1 M at 1 kHz in the potential range of -0.6 to 0.6 V. This study consists in determining the semiconductor nature and the donor density (N_D) of the prepared CuS film, as well as in estimating the flat band potential (E_{FB}) of the electrodeposited film [53]. The measured capacitance (C) can be considered a series combination of the space charge capacitance of the CuS film (C_s) which is noted (C_2 or C_3) in our case, the space charge capacitance of the formed oxides from SS (C_3), and the capacitance of the double layer SS (C_2 or C_3) [54].

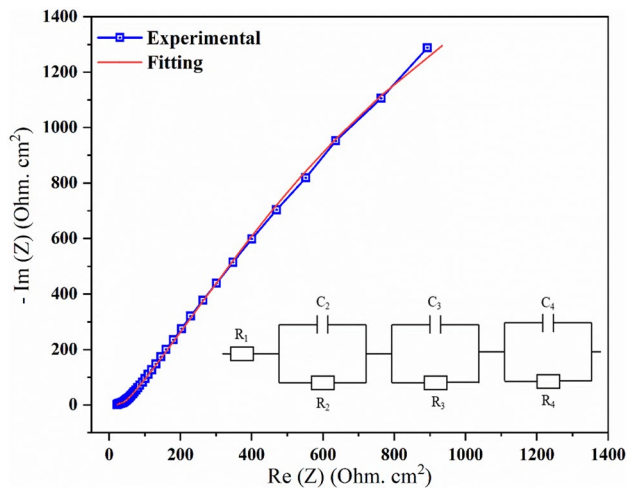


Fig. 10 Nyquist plot and equivalent circuit of the as prepared and annealed film onto stainless steel

$$\frac{1}{C} = \frac{1}{C_2} + \frac{1}{C_3} + \frac{1}{C_4} \tag{8}$$

According to the EIS study, C_2 and C_4 are very higher than C_3 . Consequently, the values of $\left(\frac{1}{C_2}\right)$ and $\left(\frac{1}{C_4}\right)$ are negligible compared to $\left(\frac{1}{C_3}\right)$ value, then the measured $\left(\frac{1}{C}\right)$ is attributed to $\left(\frac{1}{C_3}\right)$. Figure 10 shows the plot of inverse squares of space charge capacitance $\left(\frac{1}{C_s^2}\right)$ versus potential (Mott–Schottky plot).

This figure indicates a quasilinear behavior of the variation of $\left(\frac{1}{C_s^2}\right)$ with potential. According to the literature, CuS is a p-type semiconductor [19, 41, 69, 70]. However, this study indicates that Mott–Schottky plot has a positive slope corresponding to an n-type semiconductor. This result indicates that the measured $\left(\frac{1}{C_s^2}\right)$ is relative to $\left(\frac{1}{C_3^2}\right)$. This means that the observed behavior is due the oxides formed from SS substrate. To remove this ambiguity, the same analysis was carried out on stainless steel without deposit after been polarized from 1 to -1 V. This analysis confirmed that the observed behavior in Fig. 11 is due to the oxides formed from SS substrate, and this result was also reported in literature [71, 72].

In this case, the determination of donor density (N_D) and the flat band potential (E_{FB}) of the deposited film using the relation (9) [53], became relative to the stainless steel substrate. This result may be explained by the low thickness and the observed cracks in the prepared film.

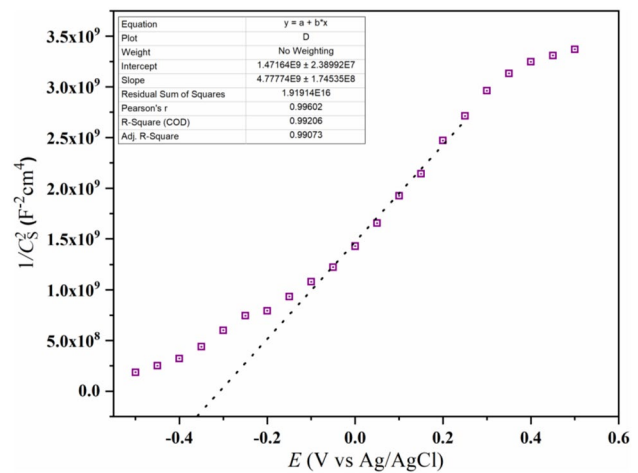


Fig. 11 Mott–Schottky plot of as prepared and annealed film onto stainless steel

$$\frac{1}{C_s^2} = \frac{2}{\epsilon_0 \epsilon_s e N_D} \left(E - E_{FB} - \frac{kT}{e} \right) \tag{9}$$

where:

- e is the electron charge (1.60×10^{-19} C)
- ϵ_0 is the permittivity of free space (8.85×10^{-12} F/m)
- $\epsilon_s = 100$ is the dielectric constant of CuS
- E is the applied potential
- k is the Boltzmann constant (1.38×10^{-23} J/K)
- T the absolute temperature

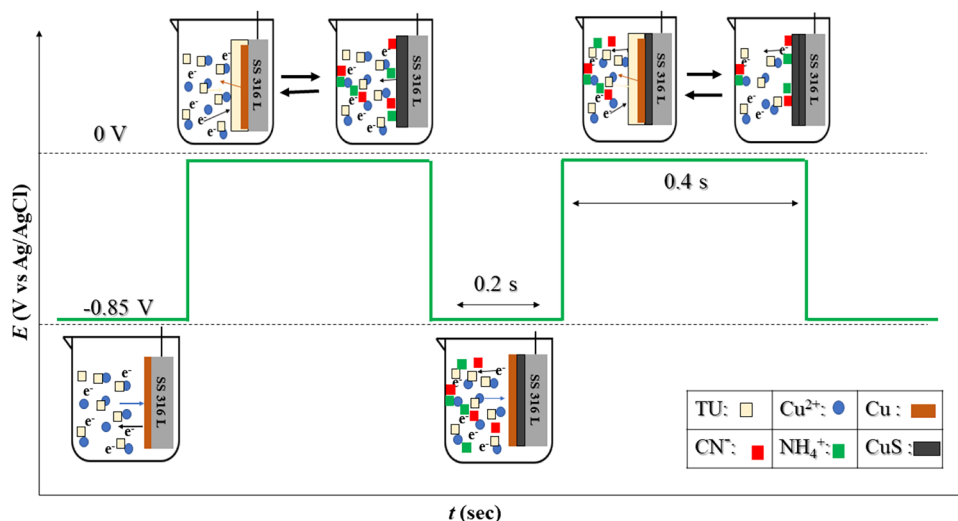
Proposed growth mechanism of CuS

The establishment of a growth mechanism of copper sulfide film performed by the pulse electrodeposition method was based on the CV studies and pulse electrodeposition study results. In this work, CuS film was obtained onto SS 316 L by applying -0.85 V for 0.2 s followed by 0 V for 0.4 s. To understand the mechanism growth of the as-prepared film, the effects of the operating parameters and the used electrolytes should be taken into consideration. As we know, TU [8, 52, 60] and sodium thiosulfate ($\text{Na}_2\text{S}_2\text{O}_3$) [51, 58] have been used as a sulfur precursor in the electrodeposition of copper sulfides. In our case, the choice of TU as a sulfur source was based on a preliminary experiment which showed that the use of $\text{Na}_2\text{S}_2\text{O}_3$ with different concentrations did not result in the formation of any film onto the SS substrate. In addition, the use of FTO as a working electrode did not result also in

Table 4 Parameters obtained by fitting the impedance spectra of the formed film

R_1 ($\Omega \times \text{cm}^2$)	C_2 (F)	R_2 ($\Omega \times \text{cm}^2$)	C_3 (F)	R_3 ($\Omega \times \text{cm}^2$)	C_4 (F)	R_4 ($\Omega \cdot \text{cm}^2$)
21.82	0.01954	1958	39.31×10^{-6}	18.43	0.01323	2868

Fig. 12 Schematic illustration of the growth mechanism of copper sulfide film



the formation of any deposit. Moreover, the application of a constant cathodic potential for the preparation of CuS results only in the formation of metallic copper onto SS and FTO. The CuS film growth by this process passes through three stages. Firstly, a metallic copper seed was grown onto SS by applying -0.85 V according to reactions (3) and (4) [8, 52]. Then, the application of 0 V consists in the dissolution of a portion of the deposited copper in the first stage following the opposite of reactions (2) and (3), the formation of copper thiourea complex at the SS surface according to reactions (5) and (7), and the formation of copper sulfide onto the SS surface according to reaction (6). In the last stage, the electrodeposited film was annealed at 200 °C to remove any organic species and to achieve the formation of a pristine CuS film. Literary, possible growth mechanism of CuS from CuSO_4 and TU using pulse electrodeposition was studied and discussed. Ghahremaninezhad et al. have proposed that CuS can be obtained onto Pt foil by this mode according to reaction (6). They also explained the whole reactions that can be carried out during the elaboration process [52]. After 8 years from the publishing of the first work, Sarma et al. have established a new growth mechanism of CuS at the same operating conditions of the first work. They proposed that CuS can be obtained from a thermal conversion of the electrodeposited copper thiourea complex [8]. In our case, CuS was obtained onto SS working electrode using the same electrodeposition mode, applied potentials and different substrate, duration of applying of E_F and E_R , and the concentration ratio of Cu(II) and TU as the two first works. As it is declared above, CuS starts its electrodeposition by Cu germination on the surface of SS at -0.85 V. Then, the electrodeposited metallic Cu reacted with TU to form CuS with some adsorbed organic species at 0 V. Finally, CN^- and NH_4^+ ions formed by TU dissolution and adsorbed onto SS surface during the electrodeposition process were

removed by annealing at 200 °C for 5 h. Figure 12 represents a schematic illustration for the growth mechanism of copper sulfide by pulse electrodeposition technique. It shows the whole stages that were carried out during the voltage applying, and the variations of the surface states against time during the electrodeposition process.

Conclusion

Copper sulfide (CuS) film has been successfully prepared onto stainless steel substrate using a pulse electrodeposition method, from a dilute copper and TU solution. The electrodeposition of CuS film was carried out by applying a forward potential of -0.85 V vs Ag/AgCl for 0.2 s and a reverse potential of 0 V vs Ag/AgCl for 0.4 s. Cyclic voltammetry study showed the chosen applied voltages for the electrodeposition process and the complexing effect of TU. It also allows us to propose the possible reactions which can be carried out in the studied system and the growth mechanism of CuS film. The pulse electrodeposition study indicated that the current density stayed the same during the elaboration process. Normal and grazing incidence XRD analysis confirmed the formation of copper sulfide. Raman analysis showed two different peaks at 270 and 473 cm^{-1} which are characteristics of the covellite CuS. SEM characterization showed that the electrodeposited and annealed film is grainy and contained some cracks. EDAX spectrum of the electrodeposited and annealed film confirmed the presence of copper and sulfur with an atomic ratio of Cu/S equal to 1.1. The annealing at 200 °C for 5 h transformed the deposited thin film to a pristine CuS without any organic constituents. Profilometry showed that the CuS film has a thickness of 7.85 ± 0.71 μm . EIS and MS analysis showed the intervention of the substrate in the modulization of the

electrolyte-thin film interface. The growth mechanism of CuS film was studied by cyclic voltammetry and shown that CuS can be obtained by this mode in three stages, the first two were purely electrochemical, and the third was a thermal step.

Acknowledgements The authors are grateful to the Center of Analyses and Characterization (CAC) of the University of Cadi Ayyad, Marrakech, Morocco.

Data availability The data used to support the findings of this study are available from the corresponding author upon request.

Declarations

Conflict of interest The authors declare no competing interests.

References

- Yang D, Liu Z (2007) One-dimensional nanostructures of silicon: synthesis, characterization and applications. *Adv Mater* 95–110
- Duan X, Huang Y, Cui Y, Wang J (2002) Indium phosphide nanowires as building blocks for nanoscale electronic and optoelectronic devices. *Nature* 261(409):1–4
- Lai CH, Lu MY, Chen LJ (2012) Metal sulfide nanostructures: synthesis, properties and applications in energy conversion and storage. *J Mater Chem* 22:19–30. <https://doi.org/10.1039/c1jm13879k>
- Guzeldir B, Saglam M, Ates A (2012) Deposition and characterization of CdS, CuS and ZnS thin films deposited by SILAR method. *Acta Physica Polonica A* 121:33–35. <https://doi.org/10.12693/APhysPolA.121.33>
- Yu Z, Du J, Guo S et al (2002) CoS thin films prepared with modified chemical bath deposition. *Thin Solid Films* 415:173–176
- Ikhioya IL, Ijabor B (2018) Growth and characterization of manganese sulphide (MnS) thin films
- El OR, Almaggoussi A, Rajira A et al (2021) Towards a stoichiometric electrodeposition of SnS. *Appl Phys A Mater Sci Process* 127:1–10. <https://doi.org/10.1007/s00339-020-04165-2>
- Sarma A, Dippel AC, Gutowski O et al (2019) Electrodeposition of nanowires of a high copper content thiourea precursor of copper sulfide. *RSC Adv* 9:31900–31910. <https://doi.org/10.1039/c9ra04293h>
- George J, Joseph KS (1983) Amorphous films of CuS. *Solid State Commun* 48:601–603. [https://doi.org/10.1016/0038-1098\(83\)90524-0](https://doi.org/10.1016/0038-1098(83)90524-0)
- Chen Y, Davoisne C, Tarascon JM, Guéry C (2012) Growth of single-crystal copper sulfide thin films via electrodeposition in ionic liquid media for lithium ion batteries. *J Mater Chem* 22:5295–5299. <https://doi.org/10.1039/c2jm16692e>
- Manivannan R, Victoria SN (2018) Preparation of chalcogenide thin films using electrodeposition method for solar cell applications – a review. *Sol Energy* 173:1144–1157. <https://doi.org/10.1016/j.solener.2018.08.057>
- Reynolds DC, Leies G, Antes LL, Marburger RE (1991) Photovoltaic effect in cadmium sulfide. *Semiconductor Devices: Pioneering Papers* 971–972. https://doi.org/10.1142/9789814503464_0139
- Chu L, Zhou B, Mu H et al (2008) Mild hydrothermal synthesis of hexagonal CuS nanoplates. *J Cryst Growth* 310:5437–5440. <https://doi.org/10.1016/j.jcrysgro.2008.09.159>
- Chen L, Yu W, Li Y (2009) Synthesis and characterization of tubular CuS with flower-like wall from a low temperature hydrothermal route. *Powder Technol* 191:52–54. <https://doi.org/10.1016/j.powtec.2008.09.007>
- Zhang J, Zhang Z (2008) Hydrothermal synthesis and optical properties of CuS nanoplates. *Mater Lett* 62:2279–2281. <https://doi.org/10.1016/j.matlet.2007.11.069>
- Patil SA, Mengal N, Memon AA et al (2017) CuS thin film grown using the one pot, solution-process method for dye-sensitized solar cell applications. *J Alloy Compd* 708:568–574. <https://doi.org/10.1016/j.jallcom.2017.03.026>
- Dhasade SS, Patil JS, Han SH et al (2013) Copper sulfide nanorods grown at room temperature for photovoltaic application. *Mater Lett* 90:138–141. <https://doi.org/10.1016/j.matlet.2012.09.013>
- Chinnadurai D, Rajendiran R, Kandasamy P (2022) Bimetallic copper nickel sulfide electrocatalyst by one step chemical bath deposition for efficient and stable overall water splitting applications. *J Colloid Interface Sci* 606:101–112. <https://doi.org/10.1016/j.jcis.2021.07.145>
- Liu J, Xue D (2009) Solvothermal synthesis of CuS semiconductor hollow spheres based on a bubble template route. *J Cryst Growth* 311:500–503. <https://doi.org/10.1016/j.jcrysgro.2008.09.025>
- Mazor H, Golodnitsky D, Burstein L, Peled E (2009) High power copper sulfide cathodes for thin-film microbatteries. *Electrochem Solid-State Lett* 12:232–235. <https://doi.org/10.1149/1.3240921>
- Chung JS, Sohn HJ (2002) Electrochemical behaviors of CuS as a cathode material for lithium secondary batteries. *J Power Sources* 108:226–231. [https://doi.org/10.1016/S0378-7753\(02\)00024-1](https://doi.org/10.1016/S0378-7753(02)00024-1)
- Jin K, Zhou M, Zhao H et al (2019) Electrodeposited CuS nanosheets on carbonized cotton fabric as flexible supercapacitor electrode for high energy storage. Elsevier Ltd
- Šetkus A, Galdikas A, Mironas A et al (2001) Properties of Cu_xS thin film based structures: Influence on the sensitivity to ammonia at room temperatures. *Thin Solid Films* 391:275–281. [https://doi.org/10.1016/S0040-6090\(01\)00995-6](https://doi.org/10.1016/S0040-6090(01)00995-6)
- Goel S, Chen F, Cai W (2014) Synthesis and biomedical applications of copper sulfide nanoparticles: From sensors to theranostics. *NANO MICRO Small* 10:631–645. <https://doi.org/10.1002/sml.201301174>
- Shen XP, Zhao H, Shu HQ et al (2009) Self-assembly of CuS nanoflakes into flower-like microspheres: synthesis and characterization. *J Phys Chem Solids* 70:422–427. <https://doi.org/10.1016/j.jpcs.2008.11.009>
- Aditya D, Sawitri RA, Diantoro M (2019) Electrical properties of tetrahedrite CuS based thermoelectric material. *Mater Today: Proc* 13:13–17. <https://doi.org/10.1016/j.matpr.2019.03.179>
- Sangamesha MA, Pushpalatha K, Shekar GL, Shamsundar S (2013) Preparation and characterization of nanocrystalline CuS thin films for dye-sensitized solar cells. *ISRN Nanomaterials* 2013:1–8. <https://doi.org/10.1155/2013/829430>
- Fu Y, Li Q, Liu J et al (2020) In-situ chemical vapor deposition to fabricate cuprous oxide/copper sulfide core-shell flowers with boosted and stable wide-spectral region photocatalytic performance. *J Colloid Interface Sci* 570:143–152. <https://doi.org/10.1016/j.jcis.2020.02.110>
- Isac A, Duta A, Kriza A et al (2007) The growth of CuS thin films by spray pyrolysis. *J Phys: Conf Ser* 61:477–481. <https://doi.org/10.1088/1742-6596/61/1/096>
- Sahoo AK, Mohanta P, Bhattacharyya AS (2015) Structural and optical properties of CuS thin films deposited by thermal co-evaporation. *IOP Conference Series: Mater Sci Eng* 73. <https://doi.org/10.1088/1757-899X/73/1/012123>
- Liao XH, Chen NY, Xu S et al (2003) A microwave assisted heating method for the preparation of copper sulfide nanorods. *J Cryst Growth* 252:593–598. [https://doi.org/10.1016/S0022-0248\(03\)01030-3](https://doi.org/10.1016/S0022-0248(03)01030-3)
- Pal M, Mathews NR, Sanchez-Mora E et al (2015) Synthesis of CuS nanoparticles by a wet chemical route and their

- photocatalytic activity. *J Nanopart Res* 17. <https://doi.org/10.1007/s11051-015-3103-5>
33. Singh A, Manivannan R, Victoria SN (2019) Simple one-pot sonochemical synthesis of copper sulphide nanoparticles for solar cell applications. *Arab J Chem* 12:2439–2447. <https://doi.org/10.1016/j.arabjc.2015.03.013>
 34. Li F, Wu J, Qin Q et al (2010) Controllable synthesis, optical and photocatalytic properties of CuS nanomaterials with hierarchical structures. *Powder Technol* 198:267–274. <https://doi.org/10.1016/j.powtec.2009.11.018>
 35. Bhosale PN, Patil SS, Desai ND et al (2018) Single step fabrication of CuS thin film via Hydrothermal route for solar cell application. *Am Inst Phys* 020029:1–6. <https://doi.org/10.1063/1.5047705>
 36. Riyaz S, Parveen A, Azam A (2016) Microstructural and optical properties of CuS nanoparticles prepared by sol–gel route. *Perspectives Sci* 8:632–635. <https://doi.org/10.1016/j.pisc.2016.06.041>
 37. Gao L, Wang E, Lian S et al (2004) Microemulsion-directed synthesis of different CuS nanocrystals. *Solid State Commun* 130:309–312. <https://doi.org/10.1016/j.ssc.2004.02.014>
 38. Zhang HT, Wu G, Chen XH (2006) Controlled synthesis and characterization of covellite (CuS) nanoflakes. *Mater Chem Phys* 98:298–303. <https://doi.org/10.1016/j.matchemphys.2005.09.024>
 39. Wang Q, Li J, Li G et al (2007) Formation of CuS nanotube arrays from CuCl nanorods through a gas-solid reaction route. *J Cryst Growth* 299:386–392. <https://doi.org/10.1016/j.jcrysgro.2006.11.304>
 40. Li B, Xie Y, Xue Y (2007) Controllable synthesis of CuS nanostructures from self-assembled precursors with biomolecule assistance. *J Phys Chem* 12181–12187
 41. Roy P, Srivastava SK (2007) Low-temperature synthesis of CuS nanorods by simple wet chemical method. *Mater Lett* 61:1693–1697. <https://doi.org/10.1016/j.matlet.2006.07.101>
 42. Dutta A, Dolui SK (2008) Preparation of colloidal dispersion of CuS nanoparticles stabilized by SDS. *Mater Chem Phys J* 112:448–452. <https://doi.org/10.1016/j.matchemphys.2008.05.072>
 43. Wu C, Shi J, Chen C et al (2008) Synthesis and optical properties of CuS nanowires fabricated by electrodeposition with anodic alumina membrane. *Mater Lett* 62:1074–1077. <https://doi.org/10.1016/j.matlet.2007.07.046>
 44. Tan C, Lu R, Xue P et al (2008) Synthesis of CuS nanoribbons templated by hydrogel. *Mater Chem Phys J* 112:500–503. <https://doi.org/10.1016/j.matchemphys.2008.06.015>
 45. Thongtem T, Phuruangrat A, Thongtem S (2009) Formation of CuS with flower-like, hollow spherical, and tubular structures using the solvothermal-microwave process. *Curr Appl Phys* 9:195–200. <https://doi.org/10.1016/j.cap.2008.01.011>
 46. Zhu L, Xie Y, Zheng X et al (2004) Fabrication of novel urchin-like architecture and snowflake-like pattern CuS. *J Cryst Growth* 260:494–499. <https://doi.org/10.1016/j.jcrysgro.2003.08.038>
 47. Ross CA (1994) Electrodeposited multilayer thin films. *Annu Rev Mater Sci* 24:159–188. <https://doi.org/10.1146/annurev.matsci.24.1.159>
 48. Suryavanshi AP, Yu MF (2006) Probe-based electrochemical fabrication of freestanding Cu nanowire array. *Appl Phys Lett* 88:86–89. <https://doi.org/10.1063/1.2177538>
 49. Pandey RK, Sahu SN, Chandra S (1996) Handbook of Semiconductor electrodeposition. Taylor & Francis, New York NY
 50. Zhang Q, Wang Q, Zhang S et al (2016) Electrodeposition in ionic liquids. *ChemPhysChem* 17:335–351. <https://doi.org/10.1002/cphc.201500713>
 51. Mahalingam T, Sanjeeviraja C (1992) Characterization of electrodeposited copper sulphide thin films. *Physica Status Solidi (a)* 129:K89–K92. <https://doi.org/10.1002/pssa.2211290232>
 52. Ghahremaninezhad A, Asselin E, Dixon DG (2011) Electrodeposition and growth mechanism of copper sulfide nanowires. *J Phys Chem C* 115:9320–9334. <https://doi.org/10.1021/jp108283z>
 53. Zakir O, Ait Karra A, Idouhli R et al (2022) Fabrication and characterization of Ag- and Cu-doped TiO₂ nanotubes (NTs) by in situ anodization method as an efficient photocatalyst. *J Solid State Electrochem*. <https://doi.org/10.1007/s10008-022-05237-4>
 54. Khadiri M, Elyaagoubi M, Idouhli R et al (2021) Characterization of Bi₂Se₃ prepared by electrodeposition. *J Solid State Electrochem* 25:479–487. <https://doi.org/10.1007/s10008-020-04807-8>
 55. Kang MS, Kim SK, Kim K, Kim JJ (2008) The influence of thiourea on copper electrodeposition: adsorbate identification and effect on electrochemical nucleation. *Thin Solid Films* 516:3761–3766. <https://doi.org/10.1016/j.tsf.2007.06.069>
 56. Hrynaskiewicz TJ, Kozłowski J, Cieszyńska E, Krogulec T (1994) Determination of NiS, NiSe and PdS formation orders during electroreduction of thiocyanate, selenocyanate and thiourea complexes of Ni(II) and Pd(II) at mercury electrodes. *J Electroanal Chem* 367:213–221. [https://doi.org/10.1016/0022-0728\(93\)03045-Q](https://doi.org/10.1016/0022-0728(93)03045-Q)
 57. Henríquez R, Froment M, Riveros G et al (2007) Electrodeposition of polyphasic films of zinc oxide sulfide from DMSO onto n-InP(100) and n-InP(111) single crystals in the presence of zinc salt, thiourea, and dissolved molecular oxygen. *J Phys Chem C* 111:6017–6023. <https://doi.org/10.1021/jp068511g>
 58. Dhasade SS, Patil JS, Kim JH et al (2012) Synthesis of CuS nanorods grown at room temperature by electrodeposition method. *Mater Chem Phys* 137:353–358. <https://doi.org/10.1016/j.matchemphys.2012.09.033>
 59. Conejeros S, Moreira IDPR, Alemany P, Canadell E (2014) Nature of holes, oxidation states, and hypervalency in covellite (cus). *Inorg Chem* 53:12402–12406. <https://doi.org/10.1021/ic502436a>
 60. Safrani T, Jopp J, Golan Y (2015) A comparative study of the structure and optical properties of copper sulfide thin films chemically deposited on various substrates. *J Mater Chem C* 3:10715–10722. <https://doi.org/10.1039/b000000x>
 61. Shuai X, Shen W, Hou Z et al (2014) A versatile chemical conversion synthesis of Cu₂S nanotubes and the photovoltaic activities for dye-sensitized solar cell. *Nanoscale Res Lett* 9:1–7. <https://doi.org/10.1186/1556-276X-9-513>
 62. Mernagh TP, Trudu AG (1993) A laser Raman microprobe study of some geologically important sulphide minerals. *Chem Geol* 103:113–127. [https://doi.org/10.1016/0009-2541\(93\)90295-T](https://doi.org/10.1016/0009-2541(93)90295-T)
 63. Munce CG, Parker GK, Holt SA, Hope GA (2007) A Raman spectroelectrochemical investigation of chemical bath deposited Cu_xS thin films and their modification. *Colloids Surf A* 295:152–158. <https://doi.org/10.1016/j.colsurfa.2006.08.045>
 64. Page M, Niitsoo O, Itzhaik Y et al (2009) Copper sulfide as a light absorber in wet-chemical synthesized extremely thin absorber (ETA) solar cells. *Energy Environ Sci* 2:220–223. <https://doi.org/10.1039/b813740d>
 65. Chaki SH, Tailor JP, Deshpande MP (2014) Covellite CuS - single crystal growth by chemical vapour transport (CVT) technique and characterization. *Mater Sci Semicond Process* 27:577–585. <https://doi.org/10.1016/j.mssp.2014.07.038>
 66. Kar P, Farsinezhad S, Zhang X, Shankar K (2014) Anodic Cu₂S and CuS nanorod and nanowall arrays: preparation, properties and application in CO₂ photoreduction. *Nanoscale* 6:14305–14318. <https://doi.org/10.1039/c4nr05371k>
 67. Bhat KS, Nagaraja HS (2021) Electrochemical hydrogen-storage performance of copper sulfide micro-hexagons. *Int J Hydrogen Energy* 46:5530–5536. <https://doi.org/10.1016/j.ijhydene.2020.11.133>
 68. Zakir O, Idouhli R, Elyaagoubi M et al (2020) Fabrication of TiO₂ nanotube by electrochemical anodization : toward photocatalytic application. *J Nanomater* 2020
 69. Roy P, Srivastava SK (2006) Hydrothermal growth of CuS nanowires from Cu - dithioamide, a novel single-source precursor. *Cryst Growth Des* 6:6–11

70. Roy P, Mondal K, Srivastava SK (2008) Synthesis of twinned CuS nanorods by a simple wet chemical method. *Cryst Growth Des* 8:1530–1534. <https://doi.org/10.1021/cg700780k>
71. Feng Z, Cheng X, Dong C et al (2010) Passivity of 316L stainless steel in borate buffer solution studied by Mott-Schottky analysis, atomic absorption spectrometry and X-ray photoelectron spectroscopy. *Corros Sci* 52:3646–3653. <https://doi.org/10.1016/j.corsci.2010.07.013>
72. Toor I-H (2011) Mott-Schottky analysis of passive films on Si containing stainless steel alloys. *J Electrochem Soc* 158:C391. <https://doi.org/10.1149/2.083111jes>

Publisher's Note Springer Nature remains neutral with regard to jurisdictional claims in published maps and institutional affiliations.

Springer Nature or its licensor (e.g. a society or other partner) holds exclusive rights to this article under a publishing agreement with the author(s) or other rightsholder(s); author self-archiving of the accepted manuscript version of this article is solely governed by the terms of such publishing agreement and applicable law.